

# Agonist–Antagonist Dilemma in Molecular Imaging: Evaluation of a Monomolecular Multimodal Imaging Agent for the Somatostatin Receptor

W. Barry Edwards, Baogang Xu, Walter Akers, Philip P. Cheney, Kexian Liang, Buck E. Rogers, Carolyn J. Anderson, and Samuel Achilefu\*

Department of Radiology, Washington University School of Medicine, St. Louis, Missouri 63110. Received August 1, 2007; Revised Manuscript Received October 4, 2007

The combination of different imaging modalities, each providing information according to its strengths, can be a powerful method for diagnosing diseases. We have synthesized a monomolecular multimodal imaging agent (MOMIA), LS172, containing a subtype-2 somatostatin receptor (SSTR2)-avid peptide (Y3-octreotate or Y3-TATE), a radiometal chelating group (DOTA) and a near-infrared (NIR) fluorescent dye (cypate). In addition to optical methods, radiolabeling LS172 with  $^{64}\text{Cu}$  and  $^{177}\text{Lu}$  provides a strategy for in vitro evaluation or in vivo multimodal imaging by positron emission tomography (PET) and single photon emission computed tomography (SPECT), respectively. Determination of the binding affinity of LS172,  $^{nat}\text{Cu}$ - and  $^{nat}\text{Lu}$ -LS172 in SSTR2-transfected A427 cells (A427-7) showed that they all displayed high binding affinity toward SSTR2 with  $K_i$  values of 0.234 nM, 11.5 nM, and 2.15 nM respectively. In contrast to cypate-labeled Y3-TATE (cytate), fluorescence microscopy showed that LS172 and  $^{nat}\text{Cu}$ -LS172 accumulate modestly in A427-7 cells by SSTR2-mediated endocytosis, in spite of their relatively high binding affinity. In vivo, the biodistribution of the SSTR2 receptor specific  $^{64}\text{Cu}$ - and  $^{177}\text{Lu}$ -LS172 in AR42J tumor-bearing rats exhibited low ( $\leq 1\%$  ID/g) accumulation in tumor tissue. Clearance from circulation was predominantly hepatobiliary ( $>90\%$  ID/liver). Both optical and radionuclear biodistribution studies showed a similar in vivo distribution profile. Surprisingly, the strong binding of LS172 to SSTR2 did not translate into high SSTR2-mediated endocytosis in cells or uptake in tumor in vivo. Considering that LS172 is a putative antagonist, the poor accumulation of the labeled MOMIAs in SSTR2 positive tumor tissue supports the paradigm that agonists with their concomitant internalization favors appreciable target tissue accumulation of receptor-specific ligands.

## INTRODUCTION

Accurate diagnosis and treatment of diseases may be achieved by integrating a multimodal imaging strategy as part of the therapeutic regimen. With the aid of fast computational methods and algorithms for image reconstruction, coregistration of diseased tissue images can yield complimentary information, thus enhancing diagnosis. For example, computed tomographic images (CT) can be coregistered with positron emission tomographic images (PET) or single photon emission computed tomography (SPECT) (1, 2). In this way, the combination of anatomical information from CT with functional information from PET or SPECT allows cancers to be staged and precisely localized.

Optical imaging is an emerging method that could act synergistically with another imaging modality. Optical imaging itself is a highly sensitive technique that can detect, in vitro as well as in vivo, minute quantities of light-emitting materials. Additionally, it uses low energy radiation in the visible or near-infrared (NIR) regions of light to assess biological processes. As the light penetrates deeper in tissues, tissue chromophores, cellular organelles, and the matrix mediate scattering and absorption of emitted light. While algorithms can deconvolute light propagation through tissues, accurate models of the complex photon migration in heterogeneous biological systems are not available. This limitation would benefit from pairing optical with another imaging modality such as PET. By coupling together an optical and a radionuclear method, the location of

a target tissue could first be confirmed by PET then monitored longitudinally by optical imaging for such changes as tumor response to therapy.

Previously, we and others have developed near-infrared fluorescent and radiolabeled monomolecular multimodal imaging agents (MOMIAs) for combined optical radionuclear small animal imaging (3–5). Typically, these MOMIAs were labeled with gamma-emitting  $^{111}\text{In}$  for scintigraphy or SPECT. These studies demonstrated the capability of obtaining coregistered images of the distribution of the MOMIAs in small animals by both fluorescence and gamma imaging methods. However, previous studies focused on using the MOMIA strategy for multimodal imaging. Interestingly, the ability of some radionuclides to emit photons for imaging and therapeutic applications provides a strategy to incorporate therapeutic radionuclides into the MOMIA concept. This can be accomplished by using  $^{177}\text{Lu}$  or  $^{64}\text{Cu}$  radiometals in MOMIA constructs.

$^{177}\text{Lu}$  ( $t_{1/2} = 6.65$  days) has gamma emissions (208 keV; 11%) for SPECT imaging and therapeutic properties ( $\beta^-$ , 497 keV; 78%). A peptide conjugate of this radiometal,  $^{177}\text{Lu}$ -DOTA-Y3-TATE, has demonstrated excellent tumor localization and good clearance properties as well as significant tumor regression in an animal model (6, 7). SPECT has many advantages as an imaging method, but PET is the current method of choice for both human and small animal molecular imaging because of its exceptionally high sensitivity and in vivo quantitative measurements of the early kinetics of drug distribution. A widely used radiometal for PET is  $^{64}\text{Cu}$  because of its convenient half-life ( $t_{1/2} = 12.7$  h) and decay properties ( $\beta^+$  (19%);  $\beta^-$  (39%)) that are suitable for PET as well as radiotherapy. Both radiometals form stable complexes with tetraazamacrocyclic

\* Corresponding author. 4525 Scott Avenue, St. Louis, MO, 63110. Phone: 314-362-8599. Fax: 314-747-5191. E-mail: achilefu@mir.wustl.edu.

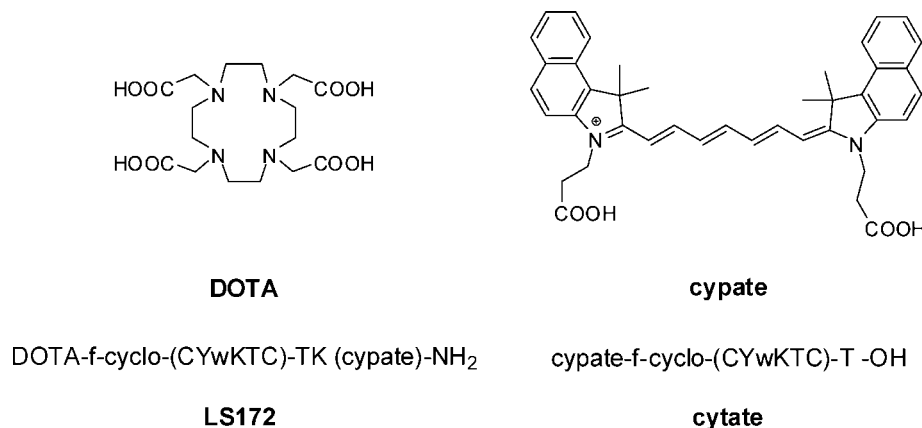


**Figure 1.** Structures of compounds used for this study. Lower case letters denote non-natural D configuration of the amino acid. DOTA and cypate are conjugated to amino groups via the carboxylic acid.

DOTA, which can be conjugated to bioactive molecules such as peptides and proteins for specific delivery to target tissue (7–10).

To take advantage of the multimodal approach, we have developed a single imaging agent that contains reporters for both optical and SPECT or PET imaging modalities as well as radiotherapeutic properties. These MOMIAs offer minimization of data analysis errors due to differences in the pharmacokinetics of two different imaging agents used for each modality, sources of error resulting from the interaction of the two imaging probes *in vivo*, and patient toxicity from repeated administration of multiple probes.

Toward this goal, we chose the well characterized somatostatin receptor subtype-2 (SSTR2) as a target and an octapeptide Y3-TATE as the targeting ligand (11, 12). Y3-TATE has been labeled with a variety of radiometals for diagnostic imaging and radiotherapy, utilizing macrocyclic chelators usually conjugated to the *N*-terminal amine (6, 7). For optical imaging, we used the near-infrared fluorescent dye cypate (13). Cypate, when conjugated to the *N*-terminus of Y3-TATE (cytate, Figure 1), was shown by optical imaging to be localized in subcutaneous SSTR2-positive tumors in rat with high selectivity (14). The NIR spectral properties of cypate match the low absorption of intrinsic naturally occurring molecules, resulting in an overall enhancement of the signal.

The three-component molecular design (receptor-avid peptide, radiometal chelate, and NIR fluorescent dye) was synthesized on solid support, where DOTA was conjugated to the *N*-terminal amine of D-Phe and cypate was conjugated to the  $\epsilon$ -amino group of a *C*-terminal lysine. The resultant MOMIA, LS172 (Figure 1), was evaluated for its ability to displace <sup>111</sup>In-DTPA-Y3-TATE in an *in vitro* binding assay. After radiolabeling with either <sup>64</sup>Cu- or <sup>177</sup>Lu-, LS172 was evaluated in a well characterized tumor model (AR42J) for *in vivo* tumor localization and clearance properties (9, 10, 15, 16). Finally, the cellular internalization of LS172 and <sup>nat</sup>Cu-LS172 was determined by fluorescence microscopy. Together, the results demonstrate that the measured high receptor binding affinity of LS172 did not translate into high cellular internalization or *in vivo* tumor uptake mediated by somatostatin receptor, suggesting that LS172 is an antagonist.

## EXPERIMENTAL PROCEDURES

**Materials.** Chemicals were obtained from Sigma-Aldrich (St. Louis, MO) unless noted differently. Amino acids were purchased from Novabiochem (San Diego, CA). Cypate and cytate were synthesized as previously described (14, 17). <sup>64</sup>Cu was produced on a CS-15 biomedical cyclotron at the Washington

University School of Medicine. <sup>177</sup>Lu was obtained from Missouri Resource Reactor (Columbia, MO). The SSTR2-positive A427-7 cells were supplied by B.E. Rogers (18). <sup>125</sup>I-SS-14 (<sup>125</sup>I-iodotyrosyl-11-somatostatin-14) was purchased from GE Healthcare (Piscataway, NJ). Protein assays were performed using the BCA assay (Pierce, Rockford, IL). Peptides were analyzed by reversed-phase HPLC (RP-HPLC) on a system consisting of a binary pumping system (Shimadzu LC-10AD, solvent A = H<sub>2</sub>O and 0.1% TFA, and solvent B = acetonitrile and 0.1% TFA), UV/vis (Shimadzu SPD-20AV), and fluorescence (Shimadzu RF-10AXL) detectors, and electrospray ionization mass spectrometer (Shimadzu LCMS-2010A).

**Peptide Synthesis.** LS172 was synthesized entirely on resin with an ACT APEX 396 peptide synthesizer by standard Fmoc protocols as previously described (14, 19). Briefly, starting with Rink Amide resin (30  $\mu$ mol), the Fmoc-protected *C*-terminal amino acid (lysine; 75  $\mu$ mol) was activated with a mixture of the coupling reagents HOBt (75  $\mu$ mol) and HBTU (75  $\mu$ mol) in the presence of DIEA (150  $\mu$ mol). Deprotection of the Fmoc protecting group was accomplished with 20% piperidine in DMF. The free carboxylic acid of tri-*t*-butyl-DOTA was coupled to the *N*-terminal amine. The orthogonal 4,4-dimethyl-2,6-dioxocyclohex-1-ylidene (Dde) protecting group, which was used to protect the  $\epsilon$ -amino group of the *C*-terminal lysine, was removed selectively with 2% hydrazine in dimethylformamide (DMF) before coupling cypate to the resultant free  $\epsilon$ -amino group via a carboxylic acid of cypate. Simultaneous removal of side-chain protecting groups and cleavage of the product from solid support was accomplished with a mixture of 95% TFA and 5% water. After lyophilization, the crude product was obtained as a green powder and purified by semipreparative HPLC. The purity of LS172 was greater than or equal to 96% after RP-HPLC purification (based on UV peak areas of 217 and 280 nm); calculated,  $M = 2169$ ; observed,  $[M]^{2+}$ , 1085;  $[M]^{3+}$ , 724. LS172 was quantified on the basis of the extinction coefficient of cypate in 20% DMSO (224,000  $M^{-1} cm^{-1}$ ) (17).

**Preparation of <sup>nat</sup>Cu- and <sup>nat</sup>Lu-LS172.** LS172 (26  $\mu$ g, 12 nmol, 0.91  $\mu$ g/ $\mu$ L, 20% DMSO) was added to reaction buffer (278  $\mu$ L, 100 mM NH<sub>4</sub>OAc, pH 4.0) containing DMSO (80  $\mu$ L). LuCl<sub>3</sub> (14 nmol, 0.4 mg LuCl<sub>3</sub>·6H<sub>2</sub>O/mL, 100 mM HCl) was added to prepare <sup>nat</sup>Lu-LS172 (20). <sup>nat</sup>Cu-LS172 was prepared similarly with CuCl<sub>2</sub> (14 nmol, 0.2 mg CuCl<sub>2</sub>·2H<sub>2</sub>O/mL, 100 mM HCl) in a more alkaline reaction buffer (279  $\mu$ L, 100 mM NH<sub>4</sub>OAc, pH 5.5) (21). The reactions were monitored by RP-HPLC (Supelco ABZ plus, C-18, 3  $\mu$ m, 4.6  $\times$  150 mm, linear gradient of 35–55%B, 20 min). <sup>nat</sup>Lu-LS172 was formed in >99% conversion and identified by LCMS, but the formation of <sup>nat</sup>Cu-LS172 was incomplete (80% conversion), as determined

by UV/vis (780 nm). Therefore, an aliquot of the reaction mixture (325  $\mu$ L) was treated with additional  $\text{CuCl}_2$  (65 nmol, 56.9  $\mu$ L, 0.2 mg  $\text{CuCl}_2 \cdot 2\text{H}_2\text{O}/\text{mL}$ , 100 mM HCl) and heated (50  $^\circ\text{C}$ , 1 h), but no additional conversion was observed.  $^{64}\text{Cu}$ -LS172 was purified by RP-HPLC (3  $\times$   $\sim$ 4  $\mu$ g portions, Supelco ABZ plus, C-18, 3  $\mu$ m, 4.6  $\times$  150 mm, linear gradient of 35–55% B, 20 min). The purity of  $^{64}\text{Cu}$ -LS172 was 95% after HPLC purification (based on UV peak area, 780 nm).  $^{177}\text{Lu}$ -LS172 was used without purification because of the complete conversion of LS172 to the metal complex.  $^{64}\text{Cu}$ -BS29, calculated, [M] = 2232; observed, [M] $^{3+}$ , 744; [M] $^{2+}$ , 1115;  $^{177}\text{Lu}$ -LS172, calculated [M] = 2169, observed, [M] $^{3+}$ , 781; [M] $^{2+}$ , 1170.

**Radiochemistry.** LS172 was radiolabeled with  $^{64}\text{Cu}$  as previously described (21). Radiochemical purity of  $^{64}\text{Cu}$ -LS172 was  $\geq$ 95% after heating (95  $^\circ\text{C}$ , 60 min), and final specific activities were 153  $\mu\text{Ci}/\mu\text{g}$  (332  $\mu\text{Ci}/\text{nmol}$ ).  $^{177}\text{Lu}$  (100  $\mu\text{Ci}$ ) was added to labeling buffer (ammonium acetate, 100 mM, pH 5.5) along with LS172 (8  $\mu$ g, 3.7 nmol) and DMSO (final concentration of 20% by volume). Purity was determined by radio-RP-HPLC (A = water, 0.1% TFA; B = acetonitrile 0.1% TFA; Vydac 201HS5415, 4.6  $\times$  150 mm, linear gradient 30% to 70% B in 10 min, 1 mL/min). Radiochemical purity of  $^{177}\text{Lu}$ -LS172 was  $\geq$ 99% after heating (80  $^\circ\text{C}$ , 80 min), and final specific activity was 12.5  $\mu\text{Ci}/\mu\text{g}$  (27  $\mu\text{Ci}/\text{nmol}$ ). For receptor-binding assays, DTPA-Y3-TATE was radiolabeled with  $^{111}\text{In}$  (100 mM  $\text{NH}_4\text{OAc}$ , pH 5.5) at a specific activity of 700  $\mu\text{Ci}/\mu\text{g}$ . Purity was  $>$ 99% (10% to 75% B, 10 min, linear gradient). Genticis acid (2,5-dihydroxy-benzoic acid) was added at a final concentration of 1 mM to prevent radiolysis (22).

**Spectral Properties of LS172.** Excitation and emission spectra were performed on a Jobin-Yvon Fluorolog 3 and absorption measurements were performed in Beckman DU-145. Stock solutions ( $\sim$ 1 mM) of indocyanine green (ICG) and LS172 were prepared in DMSO, and serial dilutions were made to obtain an absorbance level of  $\sim$ 0.02 (720 nm). The quantum yield of LS172 ( $\Phi_{\text{LS172}}$ ) relative to ICG was determined by the equation  $\Phi_{\text{LS172}} = \Phi_{\text{ICG}} (\text{slope}_{\text{LS172}}/\text{slope}_{\text{ICG}})$ , where the slope is determined from a linear regression of integrated fluorescence intensity (735 to 830 nm) versus the absorbance (720 nm) of serially diluted LS172 in DMSO (23, 24).

**Cell Culture.** The A427-7 cell line expressing the human SSTR2 receptor was maintained at 37  $^\circ\text{C}$  in a humidified atmosphere containing 5%  $\text{CO}_2$  in Eagle's minimal essential medium (EMEM) containing 4 mmol/L L-glutamine, 0.1 mM NEAA, 1.0 mM sodium pyruvate, 500  $\mu\text{g}/\text{mL}$  G418, 100 U/mL penicillin, and 10% fetal bovine serum. HEK293 cells were grown in Dulbecco's modified Eagle's medium (DMEM) containing 100 U/mL penicillin, 4 mmol/L L-glutamine, and 10% fetal bovine serum at 37  $^\circ\text{C}$  in a humidified atmosphere containing 5%  $\text{CO}_2$ .

**Fluorescence Microscopy and Internalization Assays.** A427-7 and HEK293 cells were grown in 8-well chambers and incubated in EMEM and DMEM culture media (0.2 mL/well) overnight at 37  $^\circ\text{C}$  in a humidified atmosphere containing 5%  $\text{CO}_2$ . Cytate, LS172, and  $^{64}\text{Cu}$ -LS172 were incubated with A427-7 cells at 25 or 50 nM in the presence or absence of 5  $\mu\text{M}$  Y3-TATE as a competitor. After 0, 15, 30, 60, and 90 min of incubation (37  $^\circ\text{C}$ ), the slides containing the cells were placed on ice to stop the internalization process, washed (3 $\times$ ) with PBS (4  $^\circ\text{C}$ , 1 mM  $\text{Ca}^{2+}$ ), fixed (4% paraformaldehyde), and air-dried. The fixed cells were then imaged with a confocal microscope (Olympus FV1000) equipped with excitation (775nm/50nm) and emission filters (845nm/55nm) for fluorescence detection in the NIR region. To generate values of relative fluorescence units (rfu) for internalized dye-conjugated peptides, a region of interest was generated by drawing a line (that

excluded the cell membrane) spanning the cytoplasm and transversing the region of greatest fluorescence intensity (Olympus FV10-ASW 1.4 software). The rfu are reported as an average of intensity of the drawn line. A cell was arbitrarily chosen from each corner as well as the center of the field as a representative sample ( $n = 5$ ). Because the background fluorescence was negligible, it was not subtracted from the total fluorescence.

**In Vitro Binding Assay.** The receptor binding assays were carried out as previously described (14). For the inhibition assays, varying concentrations of the competitor were incubated with  $^{111}\text{In}$ -DTPA-Y3-TATE and membranes enriched in SSTR2 receptor (A427-7, 2 h, ambient temperature). Membrane levels were adjusted so that no more than 10% of the added radioactivity was bound (2.5  $\mu\text{g}$  protein/well). To determine  $B_{\text{max}}$ , increasing concentrations of  $^{125}\text{I}$ -SS-14 were incubated with A427-7 membranes from either cultured cells or from xenografted tumors. Bound radiotracers were separated from unbound radiotracers by filtration through fiberglass filter pads (Millipore Multiscreen system). After rinsing, radioactivity in the pads was assessed by gamma counting. The data were fit by nonlinear regression to the following equation:  $Y = \text{bottom} + (\text{top} - \text{bottom}) / (1 + 10 \exp(X \log \text{IC}_{50}))$ , where  $Y$  is cpm bound and  $X$  is log concentration.  $K_i$  values were obtained with the Cheng-Prusoff equation. To determine  $K_D$  and  $B_{\text{max}}$  values, data were fit by nonlinear regression to total saturation binding with ligand depletion, where  $X$  is the amount of  $^{125}\text{I}$ -SS-14 (cpm) added, and  $Y$  is the total amount (cpm) of radiotracer bound. Nonlinear regression calculations were determined with GraphPad Prism (version 4.00 for Windows, GraphPad Software, San Diego, CA).

**Radiochemical Biodistribution of MOMIAs.** AR42J tumors were implanted bilaterally in the legs of male Lewis rats from donor rats (9). After 10–14 days, the tumors had grown  $\sim$ 1.5 to 2.0 g.  $^{64}\text{Cu}$ -LS172 was formulated in 20% DMSO in PBS by volume to prevent the adherence of the radioligand to the vessel.  $^{64}\text{Cu}$ -LS172 (4  $\mu\text{Ci}/27$  ng/12 pmol/rat,  $n = 5$ ) was administered via the tail vein. Y3-TATE (100  $\mu\text{g}/95$  nmol/rat,  $n = 4$ ) was included as a competitive dose.  $^{177}\text{Lu}$ -LS172 (6.2  $\mu\text{Ci}/500$  ng/230 pmol/rat) was formulated in 20% DMSO in PBS by volume with 10  $\mu\text{g}/\mu\text{L}$  genticis acid to prevent radiolysis. Y3-TATE (100  $\mu\text{g}/95$  nmol/rat,  $n = 5$ ) was included as a competitive dose.

**Optical Imaging and Biodistribution.** Six 4-week-old male NCR nu/nu mice were anesthetized with ketamine (87 mg/kg) and xylazine (13 mg/kg) via intraperitoneal injection. About  $5 \times 10^5$  A427-7 cells were injected subcutaneously in the right and left flanks of each mouse. Tumors were allowed to grow to 5–10 mm maximum diameter before treatment. For in vivo imaging, mice were anesthetized with a ketamine/xylazine cocktail as described above. LS172 (2 nmol in 100  $\mu\text{L}$  of 20% DMSO) was injected intravenously via the lateral tail vein, alone ( $n = 3$ ) and with a competitive dose of Y3-TATE (100  $\mu\text{g}/95$  nmol/mouse) ( $n = 2$ ). In vivo imaging of the treated mice was performed with a multimodal planar imaging system (IS4000MM Eastman Kodak Company, New Haven, CT). Broadband illumination from a 150 W halogen lamp was filtered by a 755/35 nm optical bandpass filter (Eastman Kodak Company, New Haven, CT), and the emitted light captured via cooled CCD camera after 830 wide-angle long-pass filter (e830WA, Eastman Kodak Company, New Haven, CT). Brightfield and NIR fluorescence images were collected at 1, 4, 8, and 24 h postinjection. Regions of interest (ROIs) were drawn within the areas related to the liver, kidneys, tumor, and a control region on the opposite flank for comparison of relative in vivo fluorescence distribution at each time point. After 24 h, the mice were euthanized by cervical dislocation under anesthesia. Tissue

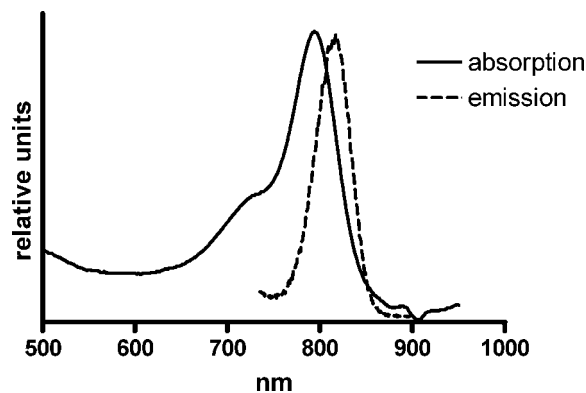


**Figure 2.** Absorption and emission spectra of LS172 (100% DMSO).  $\lambda_{\text{max,abs}} = 793$  nm,  $\lambda_{\text{max,em}} = 816$  nm, and  $\Phi_F = 0.12$ .

samples from muscle, liver, kidney, adrenal gland, pancreas, spleen, brain, skin, and tumor were harvested for ex-vivo fluorescence biodistribution imaging using the same settings as those described above.

**Statistical Methods.** Mean fluorescence intensities for the two experimental and control groups were compared with unpaired *t*-tests performed using GraphPad Prism version 4.00 for Windows (GraphPad Software, San Diego, CA).

## RESULTS

**Synthesis and Spectral Properties.** Y3-TATE is widely used to target somatostatin receptors that are up-regulated in cancer and other pathologic conditions (6, 10, 19, 20). This peptide is typically labeled with radiometal chelators or fluorescent probes for imaging applications. To design radionuclear optical MOMIA, it would be easier to incorporate a lysine residue at the *N*-terminus of the peptide to provide two amino groups for conjugating DOTA and cypate. However, in a previous study, we showed that this molecular construct can compromise the peptide's binding affinity for SSTR2 (14). In developing a macrocyclic scaffold for molecular optical imaging, we found that adding lysine to the *C*-terminus of Y3-TATE (Y3-K9-TATE) retained the binding affinity of Y3-TATE (17) and provided a second reactive group for coupling cypate at a distal position to DOTA. Thus, LS172 was prepared by conjugating DOTA and cypate at the *N*- and *C*-terminal positions of Y3-K9-TATE, respectively. To construct the entire molecule on solid support, we had to use the orthogonal Dde protecting group for lysine. This allowed us to complete the peptide synthesis and DOTA coupling before Dde removal and subsequent conjugation of cypate. The procedure is advantageous because cypate, which is unstable under basic conditions, was added toward the end of MOMIA synthesis. Thus, exposure of cypate to basic conditions was minimized, and the subsequent cleavage of the product from solid support was carried out under acidic conditions, where the NIR fluorescent dye is very stable. The structures of LS172 and other compounds used in this study are shown in Figure 1.

LS172 exhibited excellent spectral properties, including similar absorption and emission spectra to the precursor dye cypate (Figure 2). Typical of many heptamethine dyes, LS172 has a narrow Stokes shift (23 nm), but the broad excitation and emission bands allow for a wide range of wavelength choices for excitation or fluorescent detection in biological assays or in vivo imaging (25). The relative quantum yield of LS172 ( $\Phi_F = 0.12$ ) was the same as the reported quantum yield of ICG, indicating that conjugation of cypate to MOMIA did not compromise detection sensitivity.  $^{nat}\text{Cu}$ -LS172 was highly fluorescent and maintained the same fluorescent properties of the parent analogue LS172 with minimal Cu-mediated quench-

**Table 1. Heterologous Competitive Binding of  $^{111}\text{In}$ -DTPA-Y3-TATE to A427-7 Cell Membranes ( $n = 3$  for Each Data Point)<sup>a</sup>**

competitor	IC <sub>50</sub> (nM)	95% CI (nM)	K <sub>i</sub> (nM)	95% CI (nM)
cypate	1.32	0.953 to 1.83	0.234	0.169 to 0.324
Y3-TATE	2.42	1.80 to 3.25	0.427	0.318 to 0.575
SS-14	0.375	0.265 to 0.531	0.0660	0.0469 to 0.0939
LS172	8.13	5.62 to 11.7	2.03	1.14 to 2.94
$^{nat}\text{Cu}$ -LS172	45.9	33.7 to 62.4	11.5	8.40 to 15.6
$^{nat}\text{Lu}$ -LS172	8.60	4.36 to 17.0	2.15	1.09 to 4.24

<sup>a</sup> K<sub>i</sub> values were calculated from the Cheng–Prusoff equation.

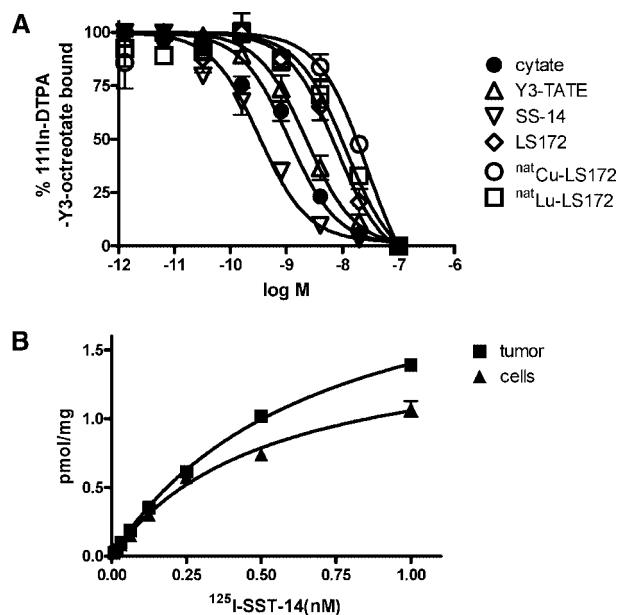


**Figure 3.** (A) Heterologous competitive inhibition assays with  $^{111}\text{In}$ -DTPA-Y3-TATE on A427-7 cell membranes. (B) Saturation binding assays of  $^{125}\text{I}$ -SS-14 on membranes from A427-7 cells harvested from xenografts (tumor) or from cultured cells (cells).

ing. Both natural and radioactive Cu and Lu were incorporated into LS172 with high radiochemical purity and specific activities for the radiometals.

**In Vitro Receptor Binding Assays.** A heterologous receptor binding assay was performed with A427-7 cell membranes, where  $^{111}\text{In}$ -DTPA-Y3-TATE was displaced by various competitors (Table 1, and Figure 3A). Utilizing a value of  $K_D = 0.13$  nM and a concentration of 0.39 nM, the Cheng–Prusoff equation was used to calculate the K<sub>i</sub> values for all of the competitors. Cypate, SS-14 and Y3-TATE display affinity for SSTR2 in the subnanomolar region. The K<sub>i</sub> values indicate that LS172 has strong affinity for SSTR2 (K<sub>i</sub> = 2.03 nM), and the complexation with lutetium had very little effect on the affinity (K<sub>i</sub> = 2.15 nM). However, the addition of copper to the chelator decreased affinity by approximately 5-fold (K<sub>i</sub> = 11.5 nM).

$^{125}\text{I}$ -SS-14 was used to assess the receptor densities of SSTR2 on xenografted and cultured A427-7 cells (Figure 3B). The xenografted cells expressed 2.3 pmol/mg (0.5 to 4.0 pmol/mg 95%CI), while the cultured cells expressed 1.0 pmol/mg (0.3 to 1.7 pmol/mg 95% CI). The K<sub>D</sub> of  $^{125}\text{I}$ -SS-14 was essentially the same ( $p < 0.05$ , F-test) for both membrane preparations (0.3 nM, 0.03 to 0.5 nM, 95% CI, cultured A427-7 cells). The nonspecific binding was ~2%.

**Internalization by Fluorescence Microscopy.** The internalization of the MOMIAs LS172 and  $^{nat}\text{Cu}$ -LS172 was evaluated by fluorescence microscopy in the near-infrared region in A427-7 and negative control HEK293 (SSTR2 negative) cells and compared with cypate. Cypate was strongly internalized in a time-dependent manner (Figures 4 and 5), and the internaliza-

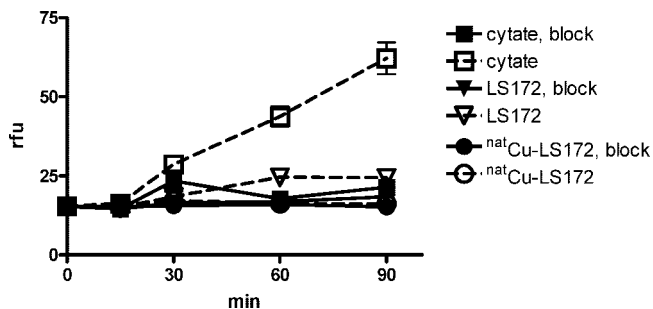


**Figure 4.** Uptake of cypate-conjugated Y3-TATE analogues determined by confocal fluorescence microscopy. Cypate-conjugated Y3-TATE analogues (25 nM) incubated (37 °C) with A427-7 cells with and without a competitive concentration of Y3-TATE (5  $\mu$ M).

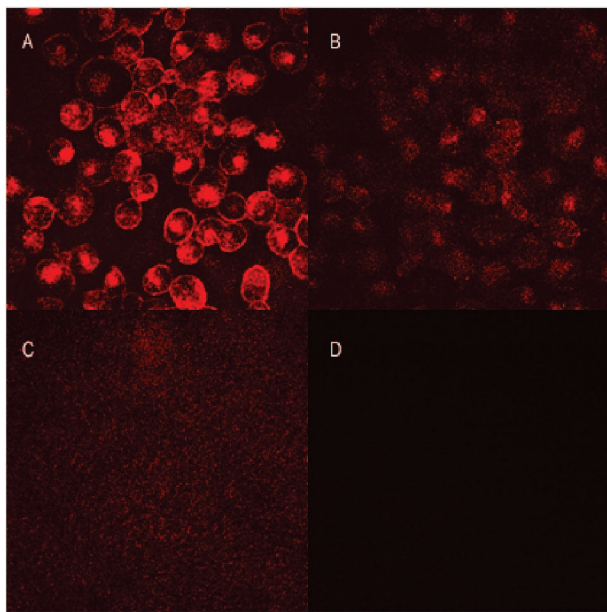


**Figure 5.** Cellular uptake of NIR dye-labeled peptides in either SSTR2-positive A427-7 cells (A and B) or SSTR2-negative HEK cells (C and D) incubated with 50 nM cypate (A and C) or LS172 (B and D) for 90 min. All of the images were normalized to the highest fluorescent intensity from the image in panel A.

tion was successfully blocked with a competitive dose of Y3-TATE. In contrast, LS172 was weakly internalized at 25 nM. A competing dose of Y3-TATE inhibited its accumulation until later time points (Figure 5). Surprisingly,  $^{nat}$ Cu-LS172 was not internalized to any significant extent in the cells (Figure 5). The apparent externalization of some of the ligands at 30 min could be attributed to an error arising from the inherently low fluorescence intensities at this early time point.

**Radiochemical Biodistribution.** Both  $^{64}$ Cu- and  $^{177}$ Lu-LS172 displayed relatively similar pharmacokinetic profiles with a rapid blood clearance of  $0.151 \pm 0.027$  and  $0.228 \pm 0.047\%$  ID/g, respectively, at 1 h postinjection (Table 2). Clearance was predominately hepatic for both  $^{64}$ Cu-LS172 ( $16.824 \pm 1.520\%$  ID/g,  $95.8 \pm 7.12\%$  ID/liver, 1 h) and  $^{177}$ Lu-LS172 ( $17.862 \pm 3.286\%$  ID/g,  $89.6 \pm 3.16\%$  ID/liver, 1 h) with relatively low kidney accumulation ( $\sim 1$  to  $2\%$  ID/g). Accumulation of activity for both radiolabeled MOMIAs in the SSTR2-positive tissues of adrenal, pituitary, pancreas, and tumor (average of left and right) were relatively low ( $\leq 1\%$  ID/g) in all cases.  $^{64}$ Cu-LS172 accumulation in tumor decreased with the coadministration of a competitive dose of Y3-TATE in the tumor ( $P < 0.05$ ), but the observed decrease in other SSTR2-positive organs was not significant. The decreases in the accumulation of  $^{177}$ Lu-LS172

**Table 2.** Biodistribution of  $^{64}$ Cu-LS172 and  $^{177}$ Lu-LS172 in AR42J Tumor Bearing Rats at 1 h, with and without the Coadministration of a Competing Dose of Y3-TATE<sup>a</sup>

tissue	$^{64}$ Cu, 1 h	$^{64}$ Cu, 1 h block	$^{177}$ Lu, 1 h	$^{177}$ Lu, 1 h block
blood	$0.151 \pm 0.027$	$0.146 \pm 0.019$	$0.228 \pm 0.047$	$0.225 \pm 0.034$
lung	$1.428 \pm 0.738$	$1.081 \pm 0.311$	$2.249 \pm 0.348$	$1.549 \pm 0.342$
liver	$16.824 \pm 1.520$	$14.547 \pm 5.227$	$17.862 \pm 3.286$	$15.478 \pm 2.829$
spleen	$8.069 \pm 1.808$	$8.013 \pm 2.997$	$5.371 \pm 1.516$	$6.413 \pm 1.734$
kidney	$1.138 \pm 0.352$	$1.256 \pm 0.101$	$1.626 \pm 0.184$	$1.600 \pm 0.202$
pituitary	$0.483 \pm 0.538$	$0.085 \pm 0.720$	$0.747 \pm 0.144^b$	$0.417 \pm 0.232$
bone	nd <sup>c</sup>	nd <sup>c</sup>	$0.225 \pm 0.086$	$0.138 \pm 0.016$
adrenals	$0.258 \pm 0.087$	$0.156 \pm 0.060$	$1.037 \pm 0.128^b$	$0.337 \pm 0.041$
pancreas	$0.148 \pm 0.027$	$0.114 \pm 0.022$	$0.307 \pm 0.054^b$	$0.138 \pm 0.015$
tumor	$0.287 \pm 0.046^b$	$0.220 \pm 0.042$	$0.319 \pm 0.049^b$	$0.139 \pm 0.025$

<sup>a</sup> Data are presented as %ID/g  $\pm$  standard deviation. <sup>b</sup>  $P < 0.05$  vs blocked (two-tailed unpaired *t*-test). <sup>c</sup> Not determined.

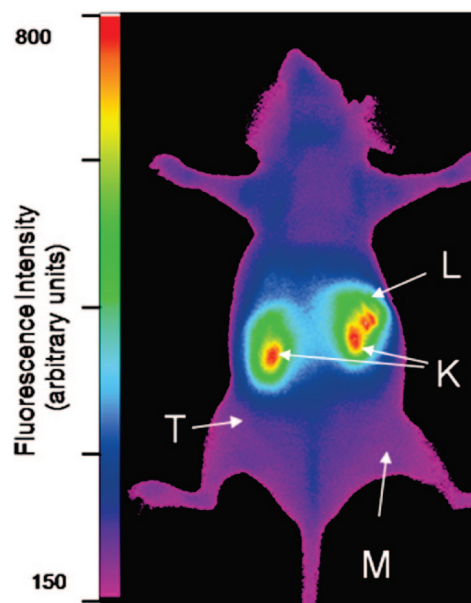


**Figure 6.** Optical Biodistribution of LS172 in nude mice xenografted with A427-7 cells (24 h). Representative fluorescence intensity image of a living mouse bearing a subcutaneous A427-7 xenograft 24 h after an injection of LS172. Liver (L), kidney (K), muscle (M), and tumor (T) regions of interest are indicated by arrows. The tumor is indistinguishable from surrounding muscle tissue by fluorescence intensity. Illumination light was selected with optical bandpass filter centered at 755 nm, and emission was captured with a cooled CCD camera after the 830 nm long-pass filter.

in SSTR2-positive tissues with the coadministration of a competitive dose of Y3-TATE were significant ( $P < 0.05$ ) in all target tissues except the bone.

**Optical Imaging.** The receptor-binding assay suggests that Cu chelation reduces the affinity of LS172. Because cypate in this MOMIA provides the NIR fluorescence signal, we were able to assess its relative biodistribution in vivo and ex vivo without metal chelation to delineate the effect of radiolabeling on LS172. Thus, we noninvasively evaluated the biodistribution of LS172 in A427-7 tumor-bearing mice at 1, 4, 8, and 24 h. LS172 rapidly accumulated in the liver and muscle tissues (Figures 6–8). At 24 h, representative tissues and organs were harvested and imaged ex-vivo to determine the relative tissue uptake of LS172 (Figure 9). In addition to the liver and kidneys, LS172 accumulated in the spleen and accounted for 35% of the fluorescence intensity relative to the liver (Figure 9). LS172 accumulation in mouse kidney was somewhat higher than that of the radiolabeled analogues in rat kidney, possibly indicating

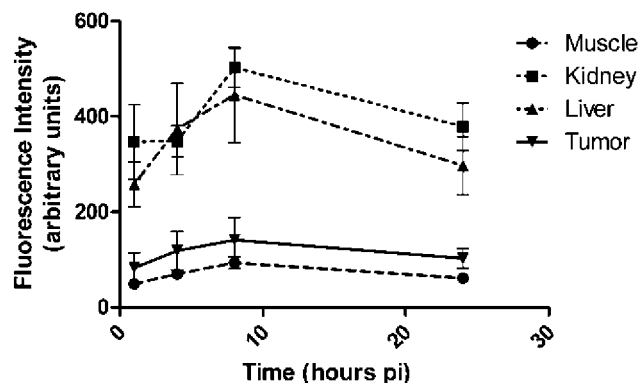


**Figure 7.** Measured fluorescence intensity of selected regions of interest that indicate the accumulation of LS172 in normal muscle, kidney, liver, and tumor tissues at specified time after an injection of contrast agent ( $n = 3$ ). Fluorescence detected in the regions of the liver and kidney was significantly higher than muscle or tumor intensity for all time points. Accumulation of contrast agent in tumor tissue paralleled that of normal tissues as determined by NIR fluorescence imaging in living mice. Error bars represent SEM.

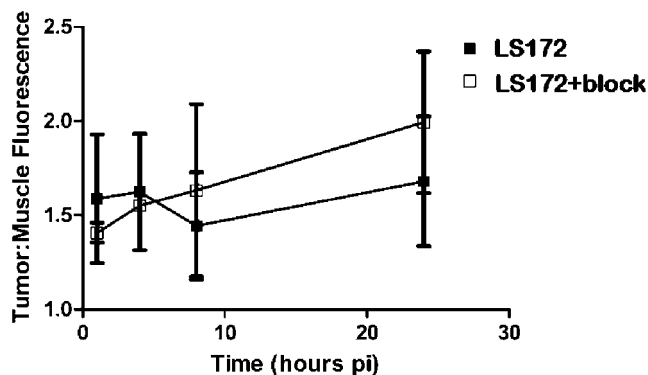


**Figure 8.** Ratios of tumor to muscle fluorescence intensities measured in living mice at given time points after an injection of LS172 ( $n = 3$ ) or LS172 with Y3-TATE as blocking agent ( $n = 2$ ). Linear regression of each data set showed that the slopes were not significantly nonzero, indicating that tumor accumulation of LS172 was not different from that of normal muscle tissue. Error bars represent SEM.

the reduction of overall charge on the DOTA upon chelation with a metal.

In spite of the high SSTR<sub>2</sub>, *in vivo* imaging did not show significant tumor accumulation of LS172 relative to normal tissue at different time points (Figure 7), and competitive inhibition with Y3-TATE did not significantly alter the tumor-to-muscle uptake ratio (Figure 8). The uptake and blood clearance profiles of LS172 in tumor-bearing A427-7 mice were similar to that of <sup>177</sup>Lu-LS172 and <sup>64</sup>Cu-LS172 in tumor-bearing AR42J rats. Inhibition studies with a competitive dose of Y3-octreotate showed that the observed uptake of LS172 in all tissues examined is attributable to nonspecific accumulation, including SSTR<sub>2</sub>-positive adrenal, pancreas, and tumor tissues (Figure 9).

## DISCUSSION

Somatostatin peptide analogues are well characterized as radioimaging and therapeutic agents for the somatostatin receptor (6, 7, 10, 15). Previous studies have shown that labeling these peptides with fluorescent dyes provides a method to image SSTR<sub>2</sub>-positive tumors in mice (14, 19, 26). The goal of this work was to determine whether a somatostatin peptide analogue, labeled with a radiometal and a NIR fluorescent dye, would localize in a receptor-specific manner to a target tissue, such as

a xenografted tumor. The somatostatin analogue was chosen on the basis of the structure of Y3-TATE, where the tetraazamacrocycle, DOTA, was conjugated to the *N*-terminal *D*-phenylalanine residue, and the near-infrared dye, cypate, was conjugated to the  $\epsilon$ -amino group of lysine at the *C*-terminus. This compound, LS172, was used for NIR fluorescence imaging or labeled with <sup>64</sup>Cu and <sup>177</sup>Lu and evaluated in tumor-bearing rats by nuclear methods. In addition, LS172 was also metallated with the natural Cu and Lu for receptor-binding studies as well as cell-uptake experiments.

In the receptor-binding studies, <sup>nat</sup>Cu-LS172 and <sup>nat</sup>Lu-LS172 were used to displace <sup>111</sup>In-DTPA-Y3-TATE (Table 1 and Figure 3A). The IC<sub>50</sub> values were converted to  $K_i$  values and compared to those of Y3-TATE, cypate, and SS14. The addition of cypate to the *N*-terminus of Y3-TATE (cypate) did not significantly change the binding affinity. However, modifications of both the *N*- and *C*-termini decreased the binding affinity of LS172 by about 10- and 5-fold relative to cypate and Y3-TATE, respectively. Moreover, while the complexation of <sup>nat</sup>Lu with DOTA had little effect on affinity, complexation of <sup>nat</sup>Cu reduced the affinity of LS172 by approximately 5-fold. In spite of the fact that the SSTR<sub>2</sub>-binding amino acid sequence of the peptide, the Phe (or Tyr)-*D*-Trp-Lys-, is relatively isolated from the termini, modifications at these sites still can affect binding. Previous studies have shown that the addition of the peptide PKKKRKY(OH) via an aminohexanoic acid linker to the *C*-terminal threonine residue of DOTA-Y3-TATE resulted in a relatively weak binding peptide when labeled with <sup>111</sup>In ( $K_D \sim 280$  nM) (27). Furthermore, DOTA-Y3-octreotide was a weaker competitor (IC<sub>50</sub> = 14 ± 2.6, SEM) toward radioiodinated SS-14 than DOTA-Y3-TATE (IC<sub>50</sub> = 1.5 ± 0.4 nM, SEM), indicating that the relatively small change from the *C*-terminal alcohol to that of the carboxylic acid can result in a nearly 10-fold increase in affinity (28). Changing the radiometal in the chelator can also affect affinity. <sup>nat</sup>Ga-DOTA-Y3-octreotide bound the SSTR<sub>2</sub> subtype with 5-fold higher affinity than the corresponding Y<sup>3+</sup> derivative. This difference was ultimately attributed to a conformational change in the *N*-terminal *D*-Phe residue of the Y<sup>3+</sup> analogue as a result of the binding of the amide *D*-Phe carbonyl oxygen in the metal-coordination sphere (29). Nevertheless, the observed affinities of <sup>nat</sup>Cu-LS172 and <sup>nat</sup>Lu-LS172 are sufficiently strong for receptor imaging, and therefore, they were radiolabeled with the corresponding radioisotopes and investigated in animal cancer models.

A well characterized tumor model, AR42J rat pancreatic xenografts, was chosen for evaluating the radiolabeled MOMIA. This model has been successful and reliable in the evaluation of a variety of radiolabeled somatostatin analogues targeted to the SSTR<sub>2</sub> with the added benefit of confirming receptor-specific uptake in SSTR<sub>2</sub>-rich organs of the adrenal, pituitary, and pancreas (9, 10, 15, 16). Previous investigations of radiolabeled somatostatin analogues showed uptakes in AR42J xenografts that ranged from low ~1% ID/g up to ~6% ID/g. For example, the accumulation of <sup>64</sup>Cu-DOTA-D-Y1-octreotate ( $K_D = 0.2$  nM) at 1 h was 1.52% ID/g and decreased to 0.468% ID/g with a competing dose of *D*-Y1-TATE (9). However, SSTR<sub>2</sub>-positive tissue uptake in pituitary, adrenal, and pancreas was 1.99, 1.37, and 1.49% ID/g, respectively, with concomitant decreases upon coadministration of a competing dose of unlabeled Y1-TATE. In another study, <sup>64</sup>Cu-TETA-Y3-TATE accumulation in AR42J xenografts at 1 h was ~1.7% ID/g with observed accumulation in pancreas and adrenals ~3.0 and 2.5% ID/g, respectively. A competing dose of Y3-TATE resulted in >90% inhibition of accumulation in these tissues (16). The observed accumulation of <sup>64</sup>Cu-LS172 in AR42J xenografts was lower, uniformly less than 1% (Table 2). Furthermore, while coadministration of a

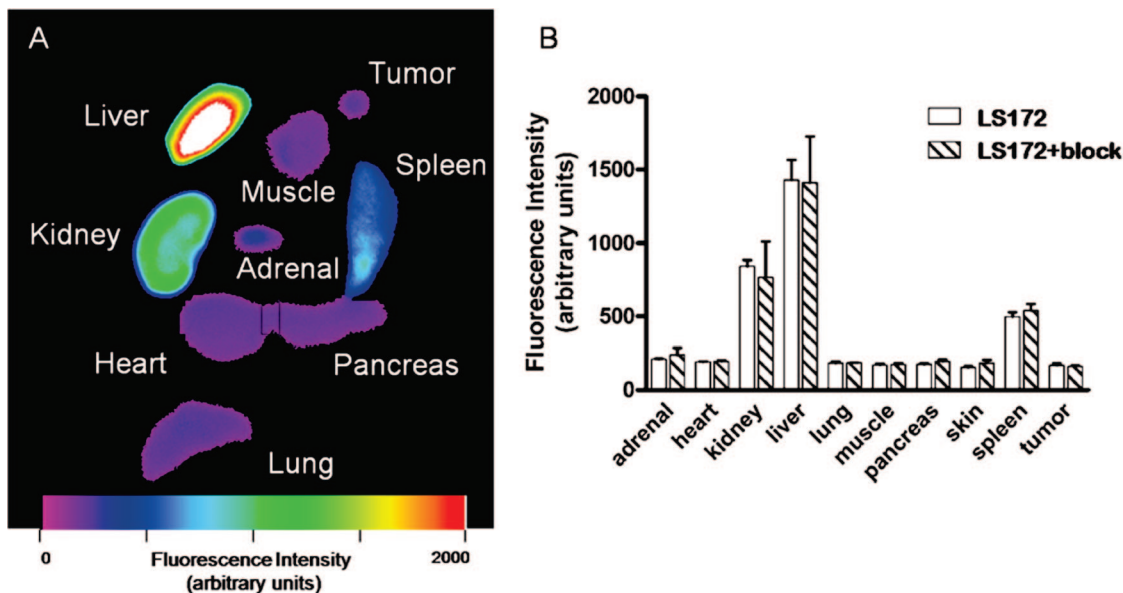


**Figure 9.** (A) Fluorescence intensity image of ex vivo organ tissues 24 h after an injection of LS172 representative of molecular probe biodistribution in mice. Liver, kidney, and spleen tissues showed high fluorescence intensity relative to that of other organs. (B) Optical biodistribution of LS172 in nude mice xenografted with A427-7 cells (24 h).

competing dose of Y3-TATE resulted in decreased uptake in all SSTR2-positive tissues, the results were significant only for the xenografted AR42J tumors ( $P < 0.05$ , two-tailed unpaired  $t$ -test). Other features of the  $^{64}\text{Cu}$ -LS172 biodistribution included relatively rapid blood clearance (1 h), predominantly hepatobiliary clearance, and relatively high spleen uptake.

The biodistribution of  $^{177}\text{Lu}$ -LS172 bore many similarities to that of  $^{64}\text{Cu}$ -LS172, including clearance pathways and rates, high spleen uptake, and lower SSTR2-positive tissue uptake ( $\leq 1\%$ ; Table 2). The exception was that SSTR2-positive tissue uptake of  $^{177}\text{Lu}$ , except for bone, was inhibited by a competitive competing dose of Y3-TATE ( $P < 0.05$ , two-tailed unpaired  $t$ -test). For comparison, the accumulation of  $^{177}\text{Lu}$ -DOTA-Y3-TATE in pancreas, adrenals, and bone (femur) at 1 and 4 h was  $\geq 10\%$  (6, 7). Competing doses of octreotide at later time points confirmed that the accumulation was receptor-specific (6). Specific activity is not considered a likely confounding factor in this study because the specific activity was 3.5-fold less ( $27 \mu\text{Ci}/\text{nmol}$ ) than the reported specific activity ( $94 \mu\text{Ci}/\text{nmol}$ ) where high accumulation in bone and pancreas were observed (7). While saturation assays on dissected AR42J xenografts were not performed to verify that they retained expression of SSTR2, the low accumulation of both  $^{64}\text{Cu}$ - and  $^{177}\text{Lu}$ -LS172 in other SSTR2-positive tissues demonstrates the poor specific uptake of LS172 in vivo. For these reasons, biodistribution of the radiolabeled LS172 at later time points was not performed in this study.

Surprised by the in vivo outcome using AR42J cells, we explored the use of an alternative cell line rich in SSTR2. We recently developed a new cell line, A427-7 (A427 clone 7) that meets our need (18). SSTR2 was transfected into A427 cells with relatively large receptor numbers ( $\sim 7.0 \text{ pmol}/\text{mg}$  protein). The transfected receptor appeared to function in identically to the wild type receptor because recent studies with SSTR2-avid  $^{64}\text{Cu}$ -TETA-octreotide showed it was internalized by A427-7 cells and had relatively high SSTR2 specific accumulation in vivo (18). Therefore, this cell line provides a method to evaluate the MOMIAs in another cell line.

Considering that the SSTR2 binding assay demonstrated that radiolabeling of LS172 with Cu reduced the affinity, we imaged the distribution and uptake of the NIR fluorescent LS172 in A427-7 tumor-bearing nude mice by fluorescence imaging.

LS172 was administered to the mice with and without a competing dose of Y3-TATE. This allowed us to determine whether the radiometal played a role in the relatively low tumor accumulations in AR 42J cells in rat.

Longitudinal, noninvasive optical imaging provided relative biodistribution data at multiple times during the 24 h after injection (Figure 7). Despite these changes, in vivo optical imaging showed that LS172 accumulation paralleled that of the radiochemical biodistribution with relatively rapid blood clearance and predominant hepatobiliary clearance with no apparent receptor-specific accumulation in the A427-7 tumor or other SSTR2-positive tissues. In vivo and ex vivo fluorescence imaging did not show significantly higher LS172 accumulation in tumor tissue relative to healthy tissues (Figures 6–9). The observed increase in kidney retention relative to radionuclear biodistribution could be attributed to species differences. Alternatively, the absence of metals in LS172 increases the net negative charge on DOTA, thereby favoring kidney uptake.

To determine whether the low accumulation of LS172 in the A427-7 cells was due to receptor downregulation, saturation assays with  $^{125}\text{I}$ -SS-14 were performed on homogenized A427-7 tumors dissected from mice. The results showed robust expression of SSTR2 ( $2.3 \text{ pmol}/\text{mg}$ ), indicating that receptor loss in the xenografts was not the cause of the low observed tumor accumulation (Figure 3B). Our observed values of SSTR2 receptor densities in the xenografted tumors were lower than the reported values (18). The difference could be attributed to differences in the method used for these measurements. Whereas we determined receptor expression level with  $^{125}\text{I}$ -SS-14, the reported values were determined with  $^{64}\text{Cu}$ -TETA-octreotide.

Recently, saturation assays with radiolabeled SSTR2 agonists and antagonists identified differing receptor densities, raising the intriguing possibility that there are differing active receptor conformations that are dependent on the radioligand (27). These observations may further explain the differing levels of receptor identified in this work relative to that previously determined (18).

Because it was unusual that ligands with such high affinity failed to localize to receptor-rich tissues in vivo, we investigated the uptake of LS172 and  $^{64}\text{Cu}$ -LS172 relative to cytate in A427-7 cells in vitro. Cytate was included as a reference because of its high SSTR2-specific accumulation in a xenografted tumor

(CA20948) in as little as 90 min (14, 19). The internalization of LS172 and  $^{64}\text{Cu}$ -LS172 by A427-7 cells was directly observed by NIR fluorescence microscopy because they are both conjugated to cypate (Figures 4 and 5). Expectedly, cypate was rapidly internalized in A427-7 cells. While LS172 also internalized, it did so at a far slower rate and to a much lower extent than cypate. Internalization of cypate and LS172 was inhibited with a competitive dose of Y3-TATE, thus demonstrating that endocytosis was mediated by the SSTR2 receptor. Lack of observed internalization of either cypate or LS172 in the SSTR2-negative HEK293 cells further confirmed the involvement of SSTR2-specific uptake in A427-7 cells. However, it should be noted that HEK293 cells express low levels of SSTR2 (30).

The hallmark of agonism is the internalization of the receptor–ligand complex (12, 15). Antagonists do not stimulate internalization. LS172, with its extremely weak internalization properties, and Cu-LS172 appear to be antagonists and cypate an agonist. Recently, the correlation between agonism, defined as the ability of a putative agonist to inhibit forskolin-stimulated cAMP production, and internalization was investigated (31). The concentration required to stimulate internalization was determined by ELISA. Both methods linked these abilities to the concentration required to obtain 50% effect ( $\text{EC}_{50}$ ). The  $\text{EC}_{50}$  ratio of internalization to cAMP inhibition of SS-28 and SS-14 was  $\sim 1$ . However, for other ligands, such as octreotide, the ratio rose to  $\sim 10$ , indicating that octreotide is 10-fold better at stimulating adenylate cyclase than at stimulating receptor internalization. These results show that inhibition of cAMP production may not be the best approach to determine the ability of an agonist to stimulate receptor internalization.

Internalization is considered a key feature for successful in vivo accumulation of the radiotracer at the target site (15). The rationale is that after binding of the radiotracer, the receptor–ligand complex internalizes into an endocytotic pathway while the unbound ligand clears from blood and nontarget tissues. Recently, a high degree of correlation between the rate of internalization of SSTR2-avid ligands in vitro and accumulation in SSTR2-enriched xenograft (AR42J) and natural organ (pancreas) in vivo was observed (10). Moreover, successful imaging and therapy with radiolabeled somatostatin analogues in humans have utilized tracers that were internalized in vitro (32, 33). Therefore, the low accumulation of LS172 and  $^{64}\text{Cu}$ -LS172 in xenografted tumors in vivo appeared to be due to a lack of internalization of these apparent antagonists, while the high receptor-specific accumulation of cypate is due to its ability to internalize.

This result stands in sharp contrast to a recent observation that an antagonist ( $^{111}\text{In}$ -DOTA-SSTR2-ANT) accumulated to a high level ( $\sim 29\%$  ID/g, 4 h) in SSTR2-positive tumor xenografts (HEK-SSTR2 transfected tumors in nude mice) (34). The accumulation exceeded that of  $^{111}\text{In}$ -DOTA-Y3-TATE ( $\sim 16\%$  ID/g, 4 h). The authors determined that  $^{111}\text{In}$ -DOTA-SSTR2-ANT was an antagonist by its inability to inhibit forskolin-stimulated cAMP production as well as by its inability to stimulate SSTR2 internalization (immunofluorescence microscopy). Part of the explanation was that the higher number of receptors identified by the antagonist (15-fold more than the agonist) offset the internalization effect. Unfortunately, the receptor concentrations were not normalized to protein weight, which makes a comparison with our current results difficult. The A427-7 cell line maintained robust expression of the SSTR2 as a xenograft, and this high expression level (2.3 pmol/mg) did not offset the lack of internalization of LS172.

In conclusion, LS172, a monomolecular multimodal imaging agent, was radiolabeled with both  $^{64}\text{Cu}$  and  $^{177}\text{Lu}$  and evaluated as an SSTR2 receptor-imaging agent by both optical and radionuclear methods in vitro and in vivo. All of the compounds

have high SSTR2 binding affinity and retained their fluorescence properties before and after labeling with metal. In spite of the high expression level of the target, LS172 along with its radiolabeled analogues,  $^{64}\text{Cu}$ - and  $^{177}\text{Lu}$ -LS172, did not accumulate in levels commensurate with their high affinity and high target expression in tumor xenografts. Moreover, accumulation in tissues endogenously expressing SSTR2 was also very low. We attribute the low accumulation to a lack of internalization of the labeled ligands in a receptor–ligand complex characteristic of successful SSTR2 imaging agents. Although the anticipated receptor-mediated accumulation in target tissues was not observed, the excellent agreement between the optical and radiochemical biodistributions demonstrates the utility of multimodal monomolecular imaging agents (MOMIAs). In addition, the quantitative radionuclear method is useful for validating data from the high throughput qualitative planar optical imaging method. Overall, high receptor binding affinity in vitro is a necessary but not sufficient criterion for selecting ligands for in vivo imaging application. The use of dual radioimaging and therapeutic radiometals provides a strategy for monitoring treatment response, initially by either PET or SPECT, followed by optical imaging at later time points.

#### ACKNOWLEDGMENT

We thank Dr. Yunpeng Ye for preparing cypate and Mr. Christopher Sherman for performing the radio-biodistribution study. This study was supported in part by the NIH (grants R33 CA100972, R01 EB1430, R21 CA123537, and R01 CA64475).

**Supporting Information Available:** Chromatograms, radiochromatograms, and mass spectral data for LS172. This material is available free of charge via the Internet at <http://pubs.acs.org>.

#### LITERATURE CITED

- (1) Gayed, I. W., Kim, E. E., Broussard, W. F., Evans, D., Lee, J., Broemeling, L. D., Ochoa, B. B., Moxley, D. M., Erwin, W. D., and Podoloff, D. A. (2005) The value of  $^{99\text{m}}\text{Tc}$ -sestamibi SPECT/CT over conventional SPECT in the evaluation of parathyroid adenomas or hyperplasia. *J. Nucl. Med.* 46, 248–252.
- (2) Jaffer, F. A., and Weissleder, R. (2005) Molecular imaging in the clinical arena. *J. Am. Med. Assoc.* 293, 855–862.
- (3) Zhang, Z., and Achilefu, S. (2005) Spectral properties of pro-multimodal imaging agents derived from a NIR dye and a metal chelator. *Photochem. Photobiol.* 81, 1499–1504.
- (4) Zhang, Z., Liang, K., Bloch, S., Berezin, M., and Achilefu, S. (2005) Monomolecular multimodal fluorescence-radioisotope imaging agents. *Bioconjugate Chem.* 16, 1232–1239.
- (5) Houston, J. P., Ke, S., Wang, W., Li, C., and Sevick-Muraca, E. M. (2005) Quality analysis of in vivo near-infrared fluorescence and conventional gamma images acquired using a dual-labeled tumor-targeting probe. *J. Biomed. Opt.* 10, 054010.
- (6) de Jong, M., Breeman, W. A., Bernard, B. F., Bakker, W. H., Schaar, M., van Gameren, A., Bugaj, J. E., Erion, J., Schmidt, M., Srinivasan, A., and Krenning, E. P. (2001) [ $^{177}\text{Lu}$ -DOTA(0),Tyr3] octreotate for somatostatin receptor-targeted radionuclide therapy. *Int. J. Cancer* 92, 628–633.
- (7) Lewis, J. S., Wang, M., Laforest, R., Wang, F., Erion, J. L., Bugaj, J. E., Srinivasan, A., and Anderson, C. J. (2001) Toxicity and dosimetry of ( $^{177}\text{Lu}$ )-DOTA-Y3-octreotate in a rat model. *Int. J. Cancer* 94, 873–877.
- (8) Breeman, W. A., de Jong, M., de Blois, E., Bernard, B. F., Konijnenberg, M., and Krenning, E. P. (2005) Radiolabelling DOTA-peptides with  $^{68}\text{Ga}$ . *Eur. J. Nucl. Med. Mol. Imaging* 32, 478–485.
- (9) Li, W. P., Lewis, J. S., Kim, J., Bugaj, J. E., Johnson, M. A., Erion, J. L., and Anderson, C. J. (2002) DOTA-D-Tyr(1)-octreotate: a somatostatin analogue for labeling with metal and

- halogen radionuclides for cancer imaging and therapy. *Bioconjugate Chem.* 13, 721–728.
- (10) Storch, D., Behe, M., Walter, M. A., Chen, J., Powell, P., Mikolajczak, R., and Macke, H. R. (2005) Evaluation of [<sup>99m</sup>Tc/EDDA/HYNIC]octreotide derivatives compared with [<sup>111</sup>In-DOTA<sub>0</sub>Tyr<sub>3</sub>, Thr<sub>8</sub>]octreotide and [<sup>111</sup>In-DTPA<sub>0</sub>]octreotide: does tumor or pancreas uptake correlate with the rate of internalization? *J. Nucl. Med.* 46, 1561–1569.
- (11) Forrer, F., Waldherr, C., Maecke, H. R., and Mueller-Brand, J. (2006) Targeted radionuclide therapy with <sup>90</sup>Y-DOTATOC in patients with neuroendocrine tumors. *Anticancer Res.* 26, 703–707.
- (12) Hofland, L. J., and Lamberts, S. W. (2003) The pathophysiological consequences of somatostatin receptor internalization and resistance. *Endocr. Rev.* 24, 28–47.
- (13) Bugaj, J. E., Achilefu, S., Dorshow, R. B., and Rajagopalan, R. (2001) Novel fluorescent contrast agents for optical imaging of in vivo tumors based on a receptor-targeted dye-peptide conjugate platform. *J. Biomed. Opt.* 6, 122–133.
- (14) Achilefu, S., Jimenez, H. N., Dorshow, R. B., Bugaj, J. E., Webb, E. G., Wilhelm, R. R., Rajagopalan, R., Johler, J., and Erion, J. L. (2002) Synthesis, in vitro receptor binding, and in vivo evaluation of fluorescein and carbocyanine peptide-based optical contrast agents. *J. Med. Chem.* 45, 2003–2015.
- (15) Hofland, L. J., Lamberts, S. W., van Hagen, P. M., Reubi, J. C., Schaeffer, J., Waaijers, M., van Koetsveld, P. M., Srinivasan, A., Krenning, E. P., and Breeman, W. A. (2003) Crucial role for somatostatin receptor subtype 2 in determining the uptake of [<sup>111</sup>In-DTPA-D-Phe<sup>1</sup>]octreotide in somatostatin receptor-positive organs. *J. Nucl. Med.* 44, 1315–1321.
- (16) Sprague, J. E., Peng, Y., Sun, X., Weisman, G. R., Wong, E. H., Achilefu, S., and Anderson, C. J. (2004) Preparation and biological evaluation of copper-64-labeled tyr<sup>3</sup>-octreotate using a cross-bridged macrocyclic chelator. *Clin. Cancer Res.* 10, 8674–8682.
- (17) Ye, Y., Li, W. P., Anderson, C. J., Kao, J., Nikiforovich, G. V., and Achilefu, S. (2003) Synthesis and characterization of a macrocyclic near-infrared optical scaffold. *J. Am. Chem. Soc.* 125, 7766–7767.
- (18) Parry, J. J., Eiblmaier, M., Andrews, R., Meyer, L. A., Higashikubo, R., Anderson, C. J., and Rogers, B. E. (2007) Characterization of somatostatin receptor subtype 2 expression in stably transfected a-427 human cancer cells. *Mol. Imaging* 6, 56–67.
- (19) Achilefu, S., Dorshow, R. B., Bugaj, J. E., and Rajagopalan, R. (2000) Novel receptor-targeted fluorescent contrast agents for in vivo tumor imaging. *Invest. Radiol.* 35, 479–485.
- (20) Breeman, W. A., De Jong, M., Visser, T. J., Erion, J. L., and Krenning, E. P. (2003) Optimising conditions for radiolabelling of DOTA-peptides with <sup>90</sup>Y, <sup>111</sup>In and <sup>177</sup>Lu at high specific activities. *Eur. J. Nucl. Med. Mol. Imaging* 30, 917–920.
- (21) Rogers, B. E., Bigott, H. M., McCarthy, D. W., Della Manna, D., Kim, J., Sharp, T. L., and Welch, M. J. (2003) MicroPET imaging of a gastrin-releasing peptide receptor-positive tumor in a mouse model of human prostate cancer using a <sup>64</sup>Cu-labeled bombesin analogue. *Bioconjugate Chem.* 14, 756–763.
- (22) Edwards, W. B., Liang, K., Xu, B., Anderson, C. J., and Achilefu, S. (2006) Synthesis and radiolabeling of a somatostatin analog for multimodal imaging. *Proc. SPIE* 6097, 609701–609708.
- (23) Demas, J. N., and Crosby, G. A. (1971) Measurement of photoluminescence quantum yields. *J. Phys. Chem.* 75, 991–1023.
- (24) Philip, R., Penzkofer, A., Baumler, W., Szeimies, R. M., and Abels, C. (1996) Absorption and fluorescence spectroscopic investigation of indocyanine green. *J. Photochem. Photobiol. A* 96, 137–148.
- (25) Ye, Y., Bloch, S., Kao, J., and Achilefu, S. (2005) Multivalent carbocyanine molecular probes: synthesis and applications. *Bioconjugate Chem.* 16, 51–61.
- (26) Becker, A., Hassenius, C., Licha, K., Ebert, B., Sukowski, U., Semmler, W., Wiedenmann, B., and Grotzinger, C. (2001) Receptor-targeted optical imaging of tumors with near-infrared fluorescent ligands. *Nat. Biotechnol.* 19, 327–331.
- (27) Cescato, R., Schulz, S., Waser, B., Eltschinger, V., Rivier, J. E., Wester, H. J., Culler, M., Ginj, M., Liu, Q., Schonbrunn, A., and Reubi, J. C. (2006) Internalization of sst<sub>2</sub>, sst<sub>3</sub>, and sst<sub>5</sub> receptors: effects of somatostatin agonists and antagonists. *J. Nucl. Med.* 47, 502–511.
- (28) Reubi, J. C., Schar, J. C., Waser, B., Wenger, S., Heppeler, A., Schmitt, J. S., and Macke, H. R. (2000) Affinity profiles for human somatostatin receptor subtypes SST<sub>1</sub>–SST<sub>5</sub> of somatostatin radiotracers selected for scintigraphic and radiotherapeutic use. *Eur. J. Nucl. Med.* 27, 273–282.
- (29) Deshmukh, M. V., Voll, G., Kuhlewein, A., Macke, H., Schmitt, J., Kessler, H., and Gemmecker, G. (2005) NMR studies reveal structural differences between the gallium and yttrium complexes of DOTA-D-Phe<sup>1</sup>-Tyr<sup>3</sup>-octreotide. *J. Med. Chem.* 48, 1506–1514.
- (30) Law, S. F., Yasuda, K., Bell, G. I., and Reisine, T. (1993) Gi<sub>α</sub>3 and G<sub>α</sub>(o) selectively associate with the cloned somatostatin receptor subtype SSTR<sub>2</sub>. *J. Biol. Chem.* 268, 10721–10727.
- (31) Liu, Q., Cescato, R., Dewi, D. A., Rivier, J., Reubi, J. C., and Schonbrunn, A. (2005) Receptor signaling and endocytosis are differentially regulated by somatostatin analogs. *Mol. Pharmacol.* 68, 90–101.
- (32) Beutler, D., Avoleto, P., Reubi, J. C., Macke, H. R., Muller-Brand, J., Merlo, A., and Kuhne, T. (2005) Three-year recurrence-free survival in a patient with recurrent medulloblastoma after resection, high-dose chemotherapy, and intrathecal Yttrium-90-labeled DOTA<sub>0</sub>-D-Phe<sup>1</sup>-Tyr<sup>3</sup>-octreotide radiolabeled peptide brachytherapy. *Cancer* 103, 869–873.
- (33) Bodei, L., Paganelli, G., and Mariani, G. (2006) Receptor radionuclide therapy of tumors: a road from basic research to clinical applications. *J. Nucl. Med.* 47, 375–377.
- (34) Ginj, M., Zhang, H., Waser, B., Cescato, R., Wild, D., Wang, X., Erchegyi, J., Rivier, J., Macke, H. R., and Reubi, J. C. (2006) Radiolabeled somatostatin receptor antagonists are preferable to agonists for in vivo peptide receptor targeting of tumors. *Proc. Natl. Acad. Sci. U.S.A.* 103, 16436–16441.